

See discussions, stats, and author profiles for this publication at: <https://www.researchgate.net/publication/316449837>

Centerline detection on partial mesh scans by confidence vote in accumulation map

Conference Paper · December 2016

DOI: 10.1109/ICPR.2016.7899829

CITATIONS
10

READS
268

4 authors, including:



Bertrand Kerautret
Université Lumière Lyon 2
83 PUBLICATIONS 671 CITATIONS

[SEE PROFILE](#)



Adrien Krähenbühl
University of Strasbourg
23 PUBLICATIONS 227 CITATIONS

[SEE PROFILE](#)



Jacques-Olivier Lachaud
Université Savoie Mont Blanc
138 PUBLICATIONS 1,794 CITATIONS

[SEE PROFILE](#)

Some of the authors of this publication are also working on these related projects:



TreeTrace [View project](#)



Digital calculus, geometric measure theory, and applications [View project](#)

Centerline Detection on Partial Mesh Scans by Confidence Vote in Accumulation Map

Bertrand Kerautret^{*†}, Adrien Krähenbühl^{*†}, Isabelle Debled-Rennesson^{*†} and Jacques-Olivier Lachaud[‡]

^{*}Université de Lorraine, LORIA, UMR 7503, Vandoeuvre-lès-Nancy, F-54506, France

[†]CNRS, LORIA, UMR 7503, Vandoeuvre-lès-Nancy, F-54506, France

[‡]LAMA (UMR CNRS 5127), Université Savoie Mont Blanc, F-73376, France

Abstract—This paper proposes an original method for extracting the centerline of 3D objects given only partial mesh scans as input data. Its principle relies on the construction of a normal vector accumulation map build by casting digital rays from input vertices. This map is then pruned according to a confidence voting rule: confidence in a point increases if this point has maximal votes along a ray. Points with high confidence accurately delineate the centerline of the object. The resulting centerline is robust enough to allow the reconstruction of the associated graph by a simple morphological processing of the confidence and a geodesic tracking. The overall process is unsupervised and only depends on a user-chosen maximal object radius. Experiments show a good behavior on standard mesh scans. Moreover, the proposed method is not only competitive with state-of-the-art methods on perfect data, but appears to be much more reliable on imperfect or damaged data, like holes, partial scans, noise, and scans from only one direction.

I. INTRODUCTION

Given some sampling of the boundary of some tubular shape, and more generally a shape with a symmetry of revolution, detecting its centerline is a classical problem in geometry processing, and is useful for shape acquisition and modeling, reverse-engineering, or control of manufactured objects. As a matter of fact, this problem is important in many other areas relying on shape or image analysis. In medicine or biology, we can cite the extraction of vessels, bronchi or brain structure as an important step to obtain geometric measurements and help to the diagnostic of numerous pathologies [1], [2]. Tubular structures can also be found in agronomic research and industry with studies of the wood structure as the knot segmentation from X-ray CT scans [3] or the bark defect detection from laser scan [4]. In the industrial context, we can cite the problem of reverse engineering of tubular metallic pieces coming from a production line of bending machines [5], [6].

There exist many methods to recover and/or analyze tubular or locally tubular structures, and most of them are designed for a particular type of input data, e.g. meshes, volumic images, point clouds, or height maps, which depends on the acquisition device (CT scans, MRI, lasers, *Kinect*®-like devices). When data is constituted of meshes, Tagliasacchi *et al.* [7] recently proposed a method which has good performance on nice mesh without holes. We will show in the experimental section that this method is considerably perturbed when dealing with partial data, which are the standard output of laser scans. We can also mention the method based on mesh contraction from Au *et al.* which shows fine results but as mentioned by

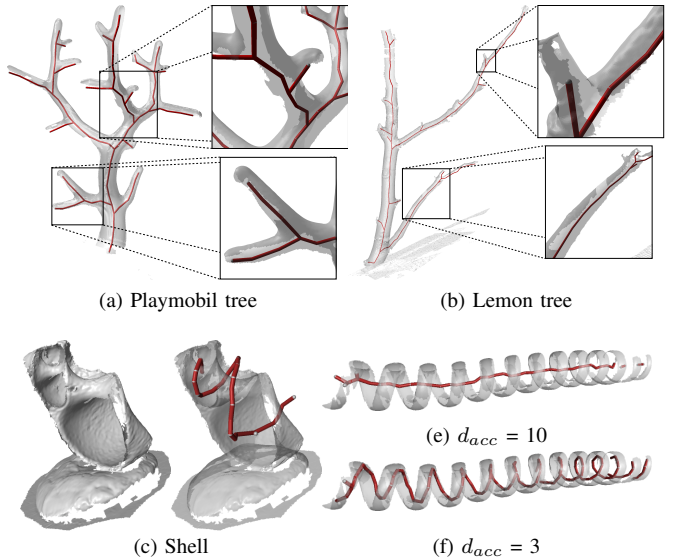


Fig. 1. Detection of the centerline of objects with a local symmetry of revolution: (a) Playmobil and (b) lemon tree scanned from one side, (c) shell with large missing parts, (d,e) phone wire without data on the inner side according to accumulation distance parameter.

the authors, the method only works for closed mesh models with manifold connectivity [8]. To overcome these limitations other work was introduced to process incomplete point cloud [9] however this method suffers from the parameters tuning. Other methods were proposed in geometry processing to work with solely point clouds as input. We can cite the methods of Lee using shrinking [10] and moving least squares [11] approaches. Bauer *et al.* proposed to recover a parametric model based on a tubular spine [5]. For digital data (generally segmented images), there are two main families of methods: methods based on the medial axis extraction, for which we can find a survey in [12] with implementations, and methods exploiting image gradient information [13], for instance the works of Hassouna *et al.* [14] or Bauer *et al.* [15] dedicated to virtual endoscopy. Unfortunately these methods are not adapted to deal with partially defined shapes (like partial scans, images with occlusions, etc), and this limitation is a serious drawback for numerous applications. Please note that all methods relying to some extent on a distance transform to input data cannot process partially sampled shapes: holes

and missing information perturbate too much the distance transform. As a consequence, methods relying on medial axis, Voronoi diagram, distance transform, thinning and skeletonization will be incorrect on such data.

Recently, we proposed a new method to detect the centerline of tubular shapes [6]. Its principle is to build a normal accumulation map from input surface data, and then to follow maxima in this map by tracking. This method is very versatile with respect to input data: it is able to extract the centerline of mesh scans, cloud of points, digital shapes in images or height maps. Its sole requirement is that a normal vector field must be associated to the input points. An optimization process was then conducted to smooth the resulting centerline approximation. The method was shown to be robust to noise and to missing data. However the method presents two major issues: its tracking step prevents it to extract branching tubular structures and its smoothing step restricts input data to tube-shaped objects with constant radius.

To overcome these limitations, we introduce in Sec. II the new notion of *accumulation confidence*, which significantly improves the quality of the centerline detection, especially for highly sparse mesh sampling (see Fig. 1). This new notion is also compatible with branching structures of variable radii of revolution. Sec. III describes a geodesic-based graph extraction algorithm following the detected centerline. Sec. IV presents several experiments and comparisons with other methods. Some applications are discussed too. Note that for space reasons we will only present results with partial mesh scans as input data, but the whole method is generic enough to process points with normals, digital images or height maps.

II. NORMAL VECTOR ACCUMULATION AND CONFIDENCE

This section presents a new notion called *accumulation confidence*, which refines the normal vector accumulation map introduced in [6]. Input data consists of a set of points with an associated normal field, for instance provided as a triangulated or quadrangulated mesh. All the proposed algorithms can be applied on an arbitrary normal vector field, independently of the initial structure: a mesh, a digital image or a point cloud. For instance if you consider digital object (resp. a point cloud), normals can be obtained by the estimator proposed by Cuel *et al.* [16] (resp. the algorithm proposed by Ran *et al.* [17]).

From now on, every step of our method is independent of the type of data. There is only one user-given parameter, called the *accumulation distance* d_{acc} . It corresponds to a length in pixel units in the discrete accumulation space. It should be chosen as $r_{max} + \epsilon$, where r_{max} denotes the maximal radius of the input tubular shape. The parameter ϵ is set $r_{max}/5$ in all our experiments. It ensures that our ray tracing algorithm reaches the object centerline even in the sample point or the normal vector direction were poorly approximated. Furthermore the gridstep of the digitized grid used in the process is determined as the average edge length of the input mesh.

A. Normal vector accumulation map

The normal vector accumulation map is built by casting digital rays from each input point in the direction of its associated inner normal vector. The length of each ray is d_{acc} . The space is thus digitized as a regular grid. Each voxel of this grid will count the number of digital rays coming from input points with length d_{acc} that cross it. The idea of the accumulation map is illustrated Fig. 2 (a,b) in the 2D case. This map remains robust even when normal vectors are poorly estimated. A 3D example of normal vector accumulation map is shown in Fig. 2 (d,e). Although this accumulation map keeps stable (but slightly diffused) maxima in presence of noise [6], the optimization process was not able to detect centerlines of objects with branches or variable radii.

B. Accumulation confidence

The *accumulation confidence* is a new notion that we introduce to estimate the reliability of an accumulation value. Let be v a voxel and v_{acc} its accumulation value, which is the number of ray segments passing through v . We define the number v_{max} as the number of rays passing through v and for which v_{acc} is the strict maximum value along the whole ray. Then, the *accumulation confidence* of v_{acc} is the ratio $v_{conf} \in [0, 1]$ such as

$$v_{conf} = v_{max}/v_{acc}.$$

The confidence is very discriminative for unwanted important accumulation values due to imprecisions on the normal vector directions. As illustrated in Fig. 2, if several voxels have a high accumulation value v_{acc} , only one has a high confidence of 1, which means that v_{acc} is the maximum value along *all* the rays voting for it. Such points are thus the exact intersection of many rays originating from input points, and corresponds to centerlines of objects with a symmetry of revolution.

C. Thresholding the accumulation confidence

Both accumulation map and confidence map could be interpreted as probabilities for each voxel to belong to the centerline of the shape. Thresholding theses maps restrict candidates to the most likely voxels, as illustrated in Fig. 3. However, it is delicate to determine a good threshold for a normal vector accumulation map. It depends both on the mesh resolution and the resolution of the discrete accumulation space, as well as the amount of noise in input data. On the contrary, thresholding the confidence map is much more intuitive, without dependence on the sampling of the input object or user choices. This is because there is always one point (and no more) that has confidence 1 at the crossing of rays. Another consequence is that the thresholding is much more robust on the confidence than on the accumulation for objects with a non constant radius (compare Fig. 3(c) and (f)). Each voxel that has a confidence value greater than some threshold is a *centerline voxel*.

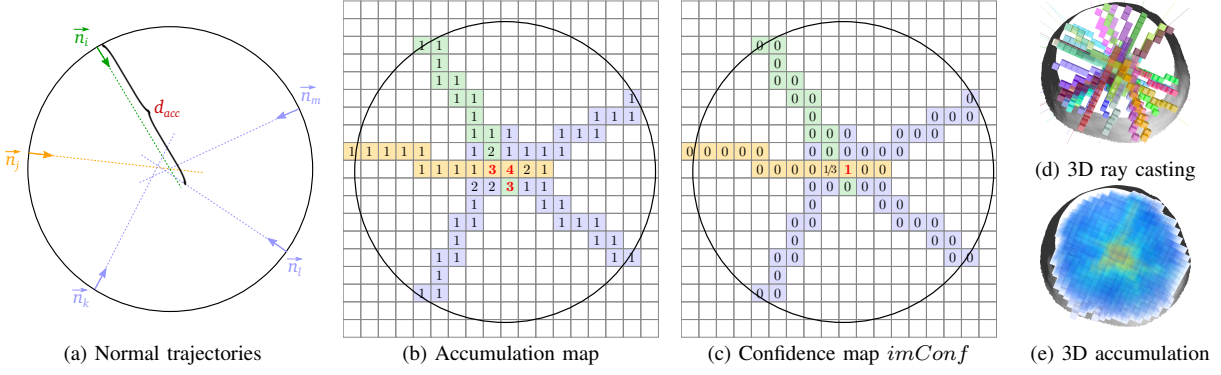


Fig. 2. Normal vector accumulation to produce the accumulation map $imAcc$ in (b). An accumulation value corresponds to the number of normal vector segments of length d_{acc} intersecting the voxel. Image (e) shows the accumulations obtained on a 3D mesh section after a ray casting (d). The corresponding confidence map $imConf$ (c) allows to discriminate the maximum values of $imAcc$. A confidence value corresponds to the ratio between the number of normal vector segments intersecting it and these for which the corresponding accumulation value is a maximum.

Algorithm 1 Compute the confidence map $imConf$ for each accumulation value of $imAcc$ from each normal vector of nvf contributing to this accumulation value.

```

1: Procedure COMPUTECONF
2: Input
3: List<Vector3D>  $nvf$  # Normal field
4: List<Point3D>  $nvo$  # Face origins
5: Image3D<Int>  $imAcc$  # Accumulation map
6: Int  $d_{acc}$  # Accumulation distance
7: Output
8: Image3D<Double>  $imConf$  # Confidence map
9: Begin
10: For  $i : 0 \rightarrow nvf.size() - 1$  do
11:   Vector3D  $norm = nvf[i]$ 
12:   Point3D  $orig, pos, maxPos = nvo[i]$ 
13:   Int  $maxAcc = 0$ 
14:   While  $orig.distanceTo(pos) < d_{acc}$  do
15:     If  $imAcc(pos) > maxAcc$  then
16:        $maxAcc = imAcc(pos)$ 
17:        $maxPos = pos$ 
18:        $pos.translate(norm)$ 
19:        $imConf(maxPos)++$ 
20:   Foreach  $pos \in imConf.domain()$  do
21:      $imConf(pos) = imConf(pos) \div imAcc(pos)$ 
22:   return  $imConf$ 
23: End
```

D. Radius estimation

We propose an algorithm to estimate the local radius at each centerline voxel from the accumulation confidence map. By construction, this estimation is available for each voxel intersected by at least one normal vector ray segment in Alg. 1. We simply attributes to each highly centerline voxel its average distance to the origins of the digital rays that cross it.

This algorithm allows by example, to reconstruct the initial shape from the radius associated to each centerline voxel. In Fig. 4, we can see two reconstructions by balls and tubes using

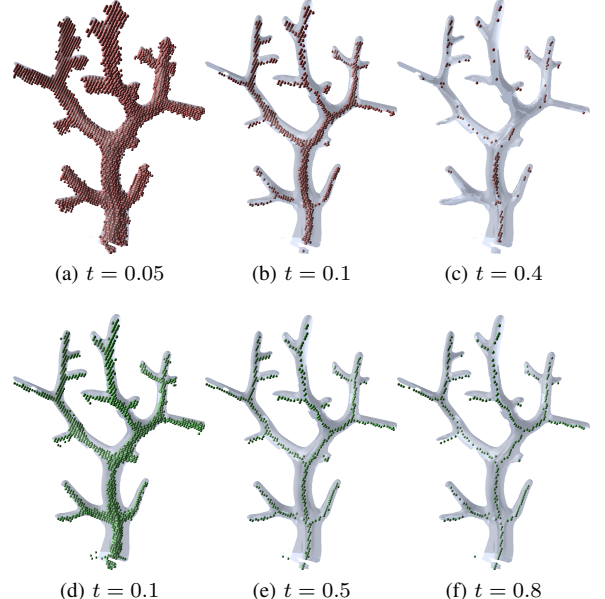
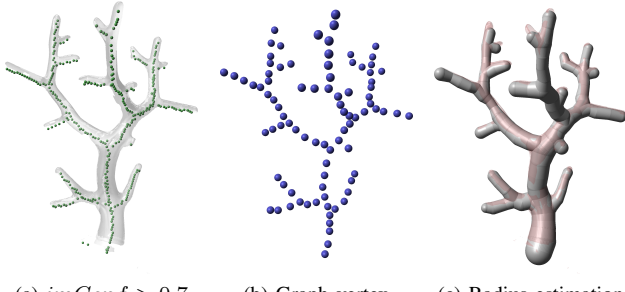


Fig. 3. Thresholding on an accumulation (a,b,c) and confidence map (d,e,f) for the manually scanned Playmobil tree. The accumulation distance is set to $d_{acc} = 6$, since the measured maximal radius r_{max} was 5.7 pixels.

the estimated radius. After the thresholding on the confidence map, we applied the graph extraction proposed in Sec. III and we drew each vertex as a ball of the estimated radius and each edge as a tube with a linear radius variation between the two linked vertex.

E. Stability of the confidence accumulation

Contrary to the normal vector accumulation map, the accumulation confidence is much more stable with respect to the threshold parameter. To evaluate this stability, we have measured the variation of the number of voxels as a function of the threshold value (associated to their number of connected components). As shown in Fig. 5, we can see that the variation of the number of voxels appears more stable for the confidence map than for the accumulation map. Related to this stability,



(a) $imConf > 0.7$ (b) Graph vertex (c) Radius estimation

Fig. 4. The thresholding of the confidence map $imConf$ (in (a)) is used as input of the graph extraction algorithm proposed in Sec. III. It produces a set of vertices (in (b)) from which we can reconstruct the initial branching object using balls and tubes (in (c)) with radii estimated as described in section Sec. II-D.

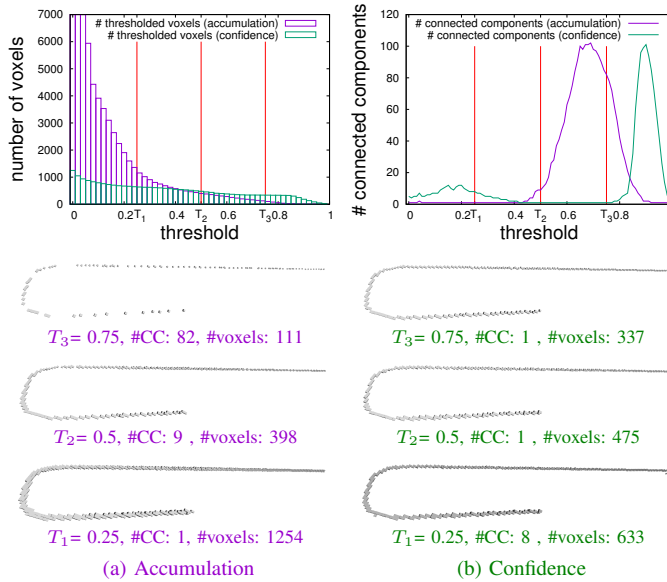


Fig. 5. Comparison of the stability towards the threshold parameters (T_1 , T_2 and T_3) and for the accumulation (left) and confidence (right) map.

the number of connected components close to one, is more frequent for the confidence map (left column of Fig. 5) than for the accumulation map (right column of Fig. 5).

This stability is a key element for designing the algorithm of graph extraction defined in the next section.

III. GEODESIC-BASED GRAPH EXTRACTION FROM CENTERLINE

The centerline detection algorithm proposed in [6] was restricted to tubular structures of constant radius without branching. The accuracy of the confidence map to delineate the centerline allows us to connect centerline voxels as a graph, thus overcoming these limits.

The proposed graph extraction algorithm takes as input the thresholded confidence map (Initial step Fig. 6). The first step consists in a morphological dilation. This connects centerline voxels. Then the voxel with maximal accumulation value defines the origin of a geodesic distance transform (Step 1). The resulting labelled voxel set is decomposed into regions

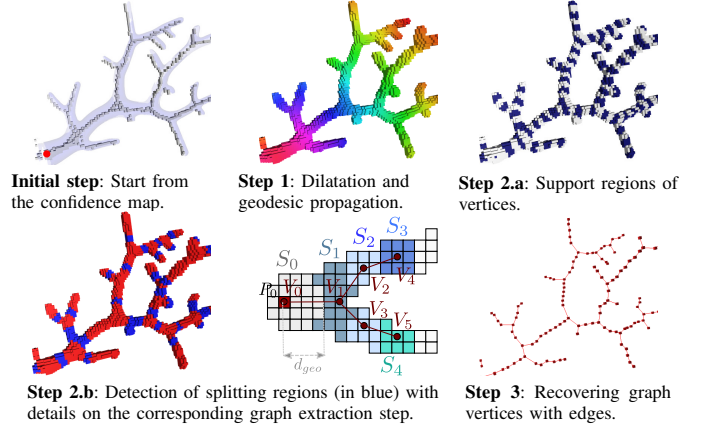


Fig. 6. The main steps of the geodesic-based graph extraction.

of similar distance (Step 2a). Each region is decomposed into its connected components: branching points corresponds to split regions (in blue Step 2b). A representative point is defined for each region to constitute the set of graph vertices (Step 3). A tracking in the geodesic distance image from the maximum accumulation value then links the vertices by simple analysis of the connectivity of ancestor regions (see the graph extraction Fig. 6). To implement this graph extraction algorithm, we used the Fast Marching Method [18] from the DGtal library [19].

The process for detecting split split process is detailed in Fig. 6. From an initial representative point P_0 the FMM propagation is iteratively applied on distance d_{geo} to remove all the points of S_0 from next candidate points. A second FMM propagation is applied from S_0 that constitutes the point set S_1 . Since there is only one connected component, this leads to only one new graph vertex V_1 . The next FFM propagation furnishes the S_2 pointset with two connected components: a graph vertex is defined for each of them, V_2 and V_3 . In this case, the process is independently repeated on each of the connected component: from V_2 the process finds V_4 and from V_3 it finds V_5 . Note that each graph vertex V_i is defined as the barycenter of the point set of the corresponding connected component of S_i .

This algorithm is based on a geodesic distance to follow at best the geometrical quasi tubular structure of the confidence map. Other generic graph reconstruction algorithms could also be adapted, for instance the metric graph based method [20]. We tried to adapt this method but the geodesic-based reconstruction provides better results in practice.

IV. RESULTS AND COMPARISONS

Fig. 7 summarized the accuracy and robustness of our method of centerline detection. It is tested on three different kinds of objects: (i) industrial metal tubes used in [6], (ii) branched objects manually scanned, leading to very partial scanned data, (iii) objects proposed in the SHREC 2011 contest [22].

Firstly, our method remains as accurate as the method of [6] on metallic tubes (see Fig. 7 (e,f,g)). The two main advantages

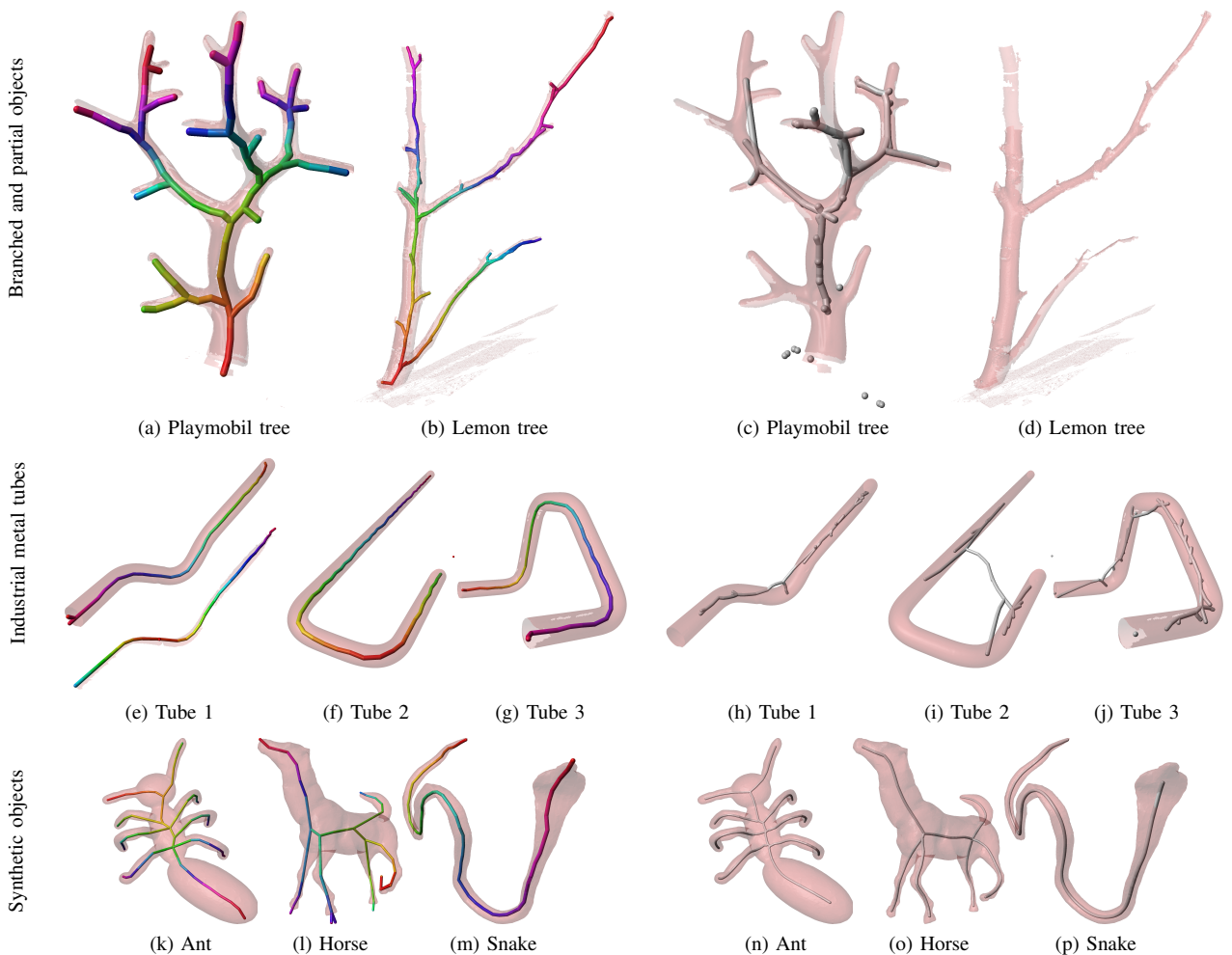


Fig. 7. In left, results of our centerline detection method from confidence in normal vector accumulation. In right, results of the mean curvature skeleton [7] on the same objects, from the CGAL implementation [21]. In the first and second lines, two trees and three industrial tubes manually scanned. In the last line, three synthetic objects of the SHREC 2011 contest [22].

TABLE I
COMPUTING TIMES OF MESH EXPERIMENTED FIG. 7

	Our method	MCS	Nb. faces
(a,c) Playmobil tree	2'20	5'08	250 873
(b,d) Lemon tree	22'47	no graph	833 128
(e,h) Tube 1	0'94	3'60	151 444
(e,h) Tube 1 partial	0'67	infinite loop	16 764
(f,i) Tube 2	1'50	5'60	230 428
(g,j) Tube 3	1'50	4'42	187 638
(k,n) Ant	2'62	0'81	19 996
(l,o) Horse	5'88	0'70	19 992
(m,p) Snake	1'02	0'45	18 926

of our method are visible on Fig. 7 (a,b). Both trees have many branches of variable radii, all acquired with a partial acquisition. Our method nicely localizes the centerlines of these trees. The precision of our method detects the branch start of trees due to bumps on the bark. The robustness to this kind of data is intrinsic to the accumulation process, comparable to a vote: it is based on the majority principle that allows the method to be independent of the number of

votes. Our method is thus extremely resilient to missing data. Last, we tested our method on data which have scarcely a local symmetry of revolution. Despite of that, our approach is competitive with the state-of-the-art method of [7], as illustrated on Fig. 7 (k,l,m), while this method is not robust to missing data. Some small defects appear for the horse hoofs with few non expected intersections, or with the non-linear ant body. However, these results are obtained without any post-processing operations.

Our results are compared to the Mean Curvature Skeleton (MCS) proposed by Tagliasacchi *et al.* [7] through the C++ implementation of the CGAL library [21]. The results are presented on the right part of Fig. 7. Even if the MCS method presents fine results on SHREC 2011 contest, we can see that the quality of the method is dramatically degraded when the scan are obtained by manual scanner acquisition. Conversely, our method performs much better on partial scans even if significant missing parts are present like on the top of the branches of lemon tree Fig. 7 (a,b). Moreover, the computing times compared in Tab. I show that the MCS is longer to

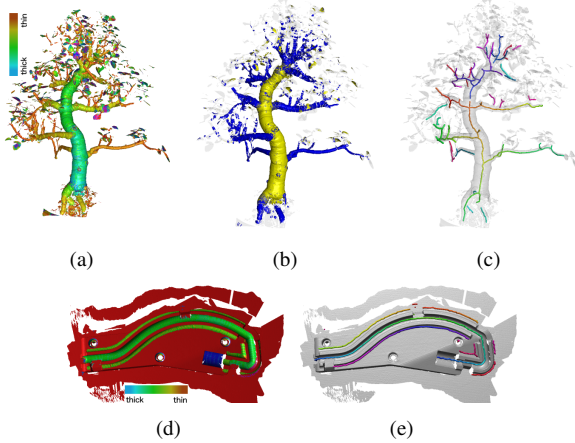


Fig. 8. Thickness estimation computed from Alg. 1 (a,d) with a segmented version (b). (c,e) show the associated centerline extraction.

compute on mesh with a consequent number of faces than our method, and is not robust on the lemon tree or the partial tube 1 with unpredictable comportments.

A. Thickness estimation

During the confidence map computation detailed in Alg. 1, we can store for each face the position of the maximal accumulation value \maxPos . By this way, we can associate to each face the value of the thickness of the tubular object and segment its tubular parts. Fig. 8 (a,d) shows this thickness estimation and (b) the segmentation into mesh faces defined according to a thickness interval selection. The last column (c,e) shows the centerline detected after a thresholding on the corresponding accumulation map.

V. CONCLUSION

The new notion of confidence on normal vector accumulation proposed an original way to detect the centerline of tube-like shapes even with imperfect or damaged data. The sole parameter is the maximal radius expected in the input data. The confidence increases the accuracy of the accumulation map. This accuracy allows us to propose a graph extraction method dealing with shapes with branching structures and radius variations. This graph extraction uses a geodesic approach combined to a connected component analysis to detect graph branchings. In addition, we proposed an estimation of the structure radii exploiting the same approach than the confidence algorithm.

Obtained results show that the method is really competitive with state-of-the-art methods on classical mesh. The major advantage of our method is its excellent robustness to partial data, which makes it particularly adapted to mesh acquired by quick manual scanning. Numerous applications can be considered: shape retrieving, mesh segmentation, geometry analysis, etc.

We are considering to improve the graph extraction approach: the radius estimation could be used in order to propose an adaptive graph extraction method. This would be

very suitable for medical applications as vessel or bronchi segmentation where important radius variations appear.

REFERENCES

- [1] D. Lesage, E. D. Angelini, I. Bloch, and G. Funka-Lea, “A review of 3d vessel lumen segmentation techniques: Models, features and extraction schemes,” *Medical Image Analysis*, vol. 13, no. 6, pp. 819–845, 2009.
- [2] O. Tankyevych, H. Talbot, N. Passat, M. Musacchio, and M. Lagneau, “Angiographic image analysis,” in *Medical Image Processing*. Springer, 2011, pp. 115–144.
- [3] A. Krähenbühl, B. Kerautret, I. Debled-Rennesson, F. Mothe, and F. Longuetaud, “Knot Segmentation in 3d CT Images of Wet Wood,” *Pattern Recognition*, 2014.
- [4] L. Thomas and L. Mili, “A robust gm-estimator for the automated detection of external defects on barked hardwood logs and stems,” *Signal Processing, IEEE Transactions on*, vol. 55, no. 7, pp. 3568–3576, 2007.
- [5] U. Bauer and K. Polthier, “Generating parametric models of tubes from laser scans,” *Computer-Aided Design*, vol. 41, no. 10, pp. 719–729, 2009.
- [6] B. Kerautret, A. Krähenbühl, I. Debled-Rennesson, and J.-O. Lachaud, “3d geometric analysis of tubular objects based on surface normal accumulation,” in *Image Analysis and Processing—ICIAP 2015*. Springer, 2015, pp. 319–331.
- [7] A. Tagliasacchi, I. Alhashim, M. Olson, and H. Zhang, “Mean curvature skeletons,” in *Computer Graphics Forum*, vol. 31. Wiley Online Library, 2012, pp. 1735–1744.
- [8] O. K.-C. Au, C.-L. Tai, H.-K. Chu, D. Cohen-Or, and T.-Y. Lee, “Skeleton Extraction by Mesh Contraction,” in *ACM SIGGRAPH*. ACM, 2008, pp. 44:1–44:10.
- [9] A. Tagliasacchi, H. Zhang, and D. Cohen-Or, “Curve skeleton extraction from incomplete point cloud,” *ACM Transactions on Graphics (TOG)*, vol. 28, no. 3, p. 71, 2009.
- [10] I.-K. Lee, “Curve reconstruction from unorganized points,” *Computer aided geometric design*, vol. 17, no. 2, pp. 161–177, 2000.
- [11] I.-K. Lee and K.-J. Kim, “Shrinking: Another method for surface reconstruction,” in *Geometric Modeling and Processing, 2004. Proceedings*. IEEE, 2004, pp. 259–266.
- [12] N. D. Cornea and D. Silver, “Curve-skeleton properties, applications, and algorithms,” *IEEE Transactions on Visualization and Computer Graphics*, vol. 13, pp. 530–548, 2007.
- [13] C. Xu and J. Prince, “Snakes, shapes, and gradient vector flow,” *IEEE Transactions on Image Processing*, vol. 7, no. 3, pp. 359–369, 1998.
- [14] M. Hassouna and A. Farag, “Variational Curve Skeletons Using Gradient Vector Flow,” *IEEE Transactions on Pattern Analysis and Machine Intelligence*, vol. 31, no. 12, pp. 2257–2274, 2009.
- [15] C. Bauer and H. Bischof, “Extracting Curve Skeletons from Gray Value Images for Virtual Endoscopy,” in *Medical Imaging and Augmented Reality*, ser. Lecture Notes in Computer Science, T. Dohi, I. Sakuma, and H. Liao, Eds. Springer Berlin Heidelberg, 2008, no. 5128, pp. 393–402.
- [16] L. Cuel, J.-O. Lachaud, and B. Thibert, “Voronoi-based geometry estimator for 3d digital surfaces,” pp. 134–149, 2014.
- [17] L. Ran, W. Wanggen, Z. Yiyuan, L. Libing, and Z. Ximin, “Normal estimation algorithm for point cloud using KD-Tree,” in *IET International Conference on Smart and Sustainable City 2013 (ICSSC 2013)*, 2013, pp. 334–337.
- [18] J. A. Sethian, “Fast marching methods,” *SIAM review*, vol. 41, no. 2, pp. 199–235, 1999. [Online]. Available: <http://pubs.siam.org/doi/abs/10.1137/S0036144598347059>
- [19] “DGtal: Digital Geometry tools and algorithms library,” <http://dgtal.org>.
- [20] M. Aanjaneya, F. Chazal, D. Chen, M. Glisse, L. Guibas, and D. Morozov, “Metric graph reconstruction from noisy data,” *International Journal of Computational Geometry & Applications*, vol. 22, no. 04, pp. 305–325, 2012. [Online]. Available: <http://www.worldscientific.com/doi/abs/10.1142/S0218195912600072>
- [21] X. Gao, S. Loriot, and A. Tagliasacchi, “Triangulated surface mesh skeletonization,” in *CGAL User and Reference Manual*, 4.8 ed. CGAL Editorial Board, 2016. [Online]. Available: <http://doc.cgal.org/4.8/Manual/packages.html#PkgMeanCurvatureSkeleton3Summary>
- [22] “Dataset for shrec 2011 - shape retrieval contest of non-rigid 3d watertight meshes,” 2011, <http://www.itl.nist.gov/iad/vug/sharp/contest/2011/NonRigid/data.html>.